

1 **Immediate-foreshocks indicating a common cascading**
2 **earthquake rupture development**

3 **Haoran Meng¹ and Wenyuan Fan¹**

4 ¹Scripps Institution of Oceanography, UC San Diego, La Jolla, CA 92093-0225, USA

5 **Key Points:**

- 6 • Abundant immediate-foreshocks are observed for 527 Ridgecrest earthquakes.
7 • Characteristics of the precursory signals do not scale with the eventual earthquake
8 magnitudes.
9 • These Ridgecrest earthquakes likely initiated as a rate-dependent cascading pro-
10 cess.

Corresponding author: Haoran Meng, h2meng@ucsd.edu

Abstract

Understanding the seismic precursors is essential for deciphering earthquake rupture physics and can aid earthquake probabilistic forecasting. With regional dense seismic arrays, we identify seismic precursors of 527 $0.9 \leq M \leq 5.4$ events of the 2019 Ridgecrest earthquake sequence, including 48 earthquakes with series of precursors. These precursors are likely immediate-foreshocks that are adjacent to the earthquakes. Their corresponding precursory signals share high resemblances with the earthquake P-waves and occur within 100 s of the P-waves. However, attributes of the immediate-foreshocks, including the amplitudes and preceding times, do not clearly scale with the eventual earthquake magnitudes. Our observations suggest that earthquake rupture may initiate in a universal fashion but evolves stochastically. This indicates that earthquake rupture development is likely controlled by fine-scale fault heterogeneities in the Ridgecrest fault system, and the final magnitude is the only difference between small and large earthquakes.

Plain Language Summary

Earthquake precursory signals can inform earthquake initiation, and some precursors can generate seismic signals. Understanding such signals have both scientific and societal implications regarding earthquake physics and seismic hazards. Using dense arrays in the Ridgecrest region, we find abundant precursory signals of 527 earthquakes that occurred within a month of the 2019 M_w 7.1 Ridgecrest earthquake. These signals are likely generated by events that immediately slipped before the earthquakes within ~ 1 km, hence immediate-foreshocks. Attributes of the precursory signal do not seem to correlate with the earthquake final magnitudes. Our observations suggest that earthquakes may initiate via similar means and it remains challenging to use such precursors to predict the their eventual magnitudes.

1 Introduction

Identifying and observing precursory signals of earthquakes have been of paramount importance because of their direct linkage with earthquake nucleation and rupture processes (e.g., Kanamori & Cipar, 1974; Ohnaka, 1992; Bouchon et al., 2013; Liu et al., 2020). Understanding such signals will offer insight of earthquake physics, but more importantly, knowledge of the signals can help hazard forecasting and mitigation (McLaskey & Yamashita, 2017; Pritchard et al., 2020). The quest of short-term earthquake prediction has been paved with failed attempts, yet remains controversial (Kanamori, 2003; Sykes et al., 1999). This is because the observed precursory signals are often reported after the earthquakes and the examinations are not systematic, leaving the physical relations between these precursors and the mainshocks elusive. In practice, these signals are often difficult to identify without prior knowledge (Kanamori, 2003; Sykes et al., 1999). However, anomalous earthquake swarms and aseismic slips preceding the 2011 Tohoku-Oki and 2014 Iquique earthquakes show promising apparent precursors that can be observed to draw connections to the final megathrust ruptures (Kato et al., 2012; Ruiz et al., 2014). Yet, the consistency of such precursory signals is unclear, which hampers their practical implementations for operational warning purposes (Mignan, 2014, 2012).

Earthquake foreshocks are one key type of possible precursors and their spatiotemporal correlation with the mainshocks suggests that they may help describe the earthquake rupture preparation process (Kato et al., 2012; Ruiz et al., 2014; Trugman & Ross, 2019). However, the general prevalence of foreshocks is less clear and the physical origin of the foreshocks is not well understood (Abercrombie & Mori, 1996; Shearer & Lin, 2009; Ellsworth & Bulut, 2018; Tape et al., 2018; Seif et al., 2019; van den Ende & Ampuero, 2020; Moutote et al., 2020). Laboratory experiments have reported a range of precursors before earthquake-like lab-quakes (Marone, 1998; McLaskey & Lockner, 2014; Tinti et al., 2016; Bolton et al., 2019; Johnson et al., 2013; Goebel et al., 2013). For ex-

ample, direct observations of multi-scale damage evolution in the failure zone (fault zone) suggest that there are fault nucleation and propagation processes, but the evolution depends on the fault stress/strength conditions, and can cause different precursors or precursors of different amplitudes for different fault systems (Renard et al., 2017, 2018). These experiments show similarities with the variability of foreshock occurrence and properties in nature (Chen & Shearer, 2013; Trugman & Ross, 2019). However, it is difficult to directly compare conventional foreshocks with laboratory experiments because of their vastly different spatiotemporal scales. Often, foreshocks are examined in a much larger spatiotemporal scale than that of the earthquake nucleation scale, leaving their relation with the mainshocks less clear.

Another type of precursors are termed nucleation phases (Spudich & Cranswick, 1984; Ellsworth & Beroza, 1995; McLaskey, 2019). Specifically, the nucleation phases are defined as accelerating aseismic slip events that are responsible for the following earthquakes (Ellsworth & Beroza, 1995; Beroza & Ellsworth, 1996; Lapusta & Rice, 2003; Kato et al., 2012; Ruiz et al., 2014). These nucleation phase investigations can be theorized as the pre-slip model (Ellsworth & Beroza, 1995; Dodge et al., 1996; McLaskey, 2019). In this model, earthquakes are nucleated by propagating aseismic slips and foreshocks are just by-products of the mainshock nucleation process. This implies that small and large earthquakes are initiated fundamentally differently and the aseismic slip size determines the nucleation length, which scales with the earthquake magnitude (Ellsworth & Beroza, 1995; Kato et al., 2012; Ruiz et al., 2014, 2017). Alternatively, numerous studies suggest that small and large earthquakes start the same way and it is difficult to predict the eventual earthquake magnitude or how the rupture would evolve based on the foreshocks or the P-wave onsets (Kilb et al., 2000; Uchide & Ide, 2010; Meier et al., 2017; Okuda & Ide, 2018; Ide, 2019; Yoon et al., 2019). These observations hint that small earthquakes can directly trigger other earthquakes by transferring stress on fault and eventually leading to the mainshock when the stress or strength condition is favorable for continuous rupture propagations, the cascade model (Ide & Aochi, 2005; McLaskey, 2019; Lui & Lapusta, 2016).

The clarity of the problem lies in robust observations of seismic precursors for earthquakes spanning a large range of magnitude but occurring in the same fault system. High-quality observations in such a relatively homogeneous geological environment are essential to track the effects of seismic precursors on the later stage ruptures. Specifically, understanding the earthquake nucleation process depends on knowing slip events shortly preceding the earthquakes, the immediate-foreshocks. We define immediate-foreshocks as slip events that can generate highly similar P-waves (precursory signals) as those of the mainshocks and are within a few folds of the mainshock rupture-dimension. We further require the immediate-foreshocks to occur within 100 seconds to ensure that the earthquakes are near-instantaneous responses of the immediate-foreshocks. In this study, we systematically investigate such immediate-foreshocks for 13,895 $0.5 \leq M \leq 5.4$ Ridgecrest earthquakes from 7 July 2019 to 6 August 2019 that were reported in Southern California Earthquake Data Center (SCEDC; Hutton et al., 2010). We find 527 earthquakes with clear precursory signals preceding P-waves generated by the immediate-foreshocks and these earthquakes are uniformly distributed across the whole fault system. These immediate-foreshocks suggest one type of common precursors preceding the Ridgecrest earthquakes, providing field observations that may bridge the conventional foreshocks and the laboratory precursors.

2 6 July 2019 M_w 5.4 Ridgecrest Earthquake

The 2019 Ridgecrest earthquake sequence, including a M_w 6.4 foreshock and a M_w 7.1 mainshock, provides an excellent opportunity to investigate the earthquake nucleation process (Figure 1a). The earthquake sequence was well recorded by regional broadband seismic networks and a number of rapid response campaign deployments soon after the

foreshock on 4 July 2019 (Cochran et al., 2020; Ross et al., 2019). In particular, multiple three-component nodal arrays (deployed after 7 July 2019 for a month) enable investigations of moderate to small magnitude earthquakes in detail (Catchings et al., 2020). In total, 13,895 earthquakes with magnitudes (M) ranging from 0.5 to 5.4 have been detected and located for the sequence (SCEDC; Hutton et al., 2010) during the deployment of the nodal array. SCEDC uses a few different magnitude scales, including moment magnitudes for larger events and local magnitudes for smaller events. The rich dataset offers an ideal natural laboratory to examine the spatiotemporal evolution of a complete earthquake sequence at an unprecedented resolution (Cochran et al., 2020; Huang et al., 2020).

Located in between the foreshock and the mainshock, a 6 July 2019 M_w 5.4 earthquake has a clear immediate-foreshock (referred as E1 in Figures 1b, S1, and S2). The seismic records are band-pass filtered at 0.5 to 20.0 Hz with a causal 2nd-order Butterworth filter to avoid possible artifacts. There are signals arriving at stations 0.8 to 1.2 s prior to the P-wave, but they are 20 times smaller in amplitude on average. These signals share high resemblance with the P-waves, and the onsets of both phases can be fit by scaling the records of a M 3.7 earthquake that is 1.5 km away from the hypocenter (SCEDC catalog; Hutton et al., 2010). We further implement the records of the M 3.7 earthquake as empirical Green's functions (eGfs) to remove the path effects to obtain the apparent source time functions (ASTFs) of the M_w 5.4 earthquake for both P- and S-waves (McGuire, 2004; Fan & McGuire, 2018; Meng et al., 2020). The ASTFs show that there are at least two distinct subevents constituting the M_w 5.4 earthquake: the first subevent (E1) as the immediate-foreshock released about 4.8% of the total seismic moment (equivalent to a M_w 4.5 earthquake), while the second subevent (E2) occurred about 0.8 s later and released the remaining moment (Figure 1b and S2).

To test the robustness of the immediate-foreshock (subevent E1), we taper the ASTFs of E1 to zero (Figure S2a) and compute synthetic seismograms with only ASTFs of E2. The synthetics cannot explain the waveforms before the P-wave arrivals (Figure S2d), confirming the immediate-foreshock. The ASTFs also show that the earthquake ruptured towards the northeast direction and the centroid locations of the two subevents are 1.1 km apart (Figure S3). With a second moments analysis (McGuire, 2017; Meng et al., 2020, Text S1), we find that the subevent E2 likely ruptured 1.3 and 1.0 km along the strike and dip directions, respectively. We further compute the strain-tensor perturbations on the fault plane generated by E1 from the numerical spatial derivatives of the displacement field, with which we then use the Hooke's law to obtain the stress perturbations (Text S1). The subevent E2 is situated in a region where both static and dynamic stress perturbations from the immediate-foreshock exceed 0.1 MPa (Figure 1b), promoting an instantaneous slip event in the area (Figure S3). Our source model shows an evolving rupture process that the immediate-foreshock cascadingly nucleated the sequential stage rupture, E2, through a stress-triggering process. This confirms that E1 is a precursor of E2 and its seismic signals are precursory signals.

3 Abundant Immediate-foreshocks

To understand the prevalence of such nucleation process, we systematically investigate immediate-foreshocks of other earthquakes of the 2019 Ridgecrest sequence. We find that similar seismic precursory signals are a common feature of 527 Ridgecrest earthquakes, indicating abundant immediate-foreshocks (Figure 1a). For example, similar immediate-foreshocks are observed for a M 3.9 earthquake that is 2.7 km away from the M_w 5.4 event, and the P waveforms of the M 3.9 earthquake are almost identical to the P-wave onsets of the M_w 5.4 subevents (Figure 2). Further, clear immediate-foreshocks can be identified for earthquakes as small as M 0.9 (Figure 2). We observe abundant yet diverse immediate-foreshocks of earthquakes spanning five magnitudes in a single 40-km-long fault system (Figures 1a and 3).

165 We identify these precursory signals by autocorrelating 0.5 to 1.0 s long P-waves
 166 with waveforms that precede the P-waves by 100 s. The autocorrelation is independently
 167 performed for all stations within 30 km of the event epicenter (Text S2). For example,
 168 a precursory signal (indicating an immediate-foreshock) is detected for a $M \leq 3.5$ earth-
 169 quake when the average autocorrelation coefficient exceeds 0.8 for more than 10 stations
 170 and these stations are from a minimum azimuthal range of 180° . For a detected immediate-
 171 foreshock, we document the amplitude ratios and the preceding times (differential time
 172 from the autocorrelation procedure) between the precursory signals and the P-waves (Fig-
 173 ure 2 and see Text S2). The immediate-foreshock is further examined by requiring the
 174 measured preceding time distribution to have a standard deviation that is less than 0.01 s
 175 for $M \leq 3.5$ earthquakes (Text S2). This quality control procedure assures that the immediate-
 176 foreshocks generating the precursory signals are adjacent to their mainshocks and they
 177 share the same focal mechanism, although the rupture details remain unresolved due to
 178 the data limitation. Finally, our procedure rules out the possibility of the detected pre-
 179 cursory signals as the fault zone head waves because of a lack of systematic phase move-
 180 outs for sensors across the fault zone (Figures S4 and S5) (Ben-Zion & Malin, 1991; Ben-
 181 Zion et al., 1992).

182 In total, we examine 13,895 $0.5 \leq M \leq 5.4$ earthquakes in the Ridgecrest re-
 183 gion that are reported in the SCEDC catalog (Hutton et al., 2010) and find that 527 events
 184 with immediate-foreshocks can be robustly identified (Table S1), out of which the M_w 5.4
 185 earthquake preceded the M_w 7.1 earthquake while the remaining events were aftershocks
 186 of the M_w 7.1 earthquake. The lack of events with immediate-foreshocks prior to the M_w 7.1
 187 earthquake (6 July 2019) is likely due to a data deficiency as the nodal arrays on the fault
 188 zone were only deployed after 7 July 2019 (Catchings et al., 2020). Our analysis relies
 189 on the near-fault dataset and an autocorrelation method to study the earthquake prepara-
 190 tion process. Therefore, we do not analyze the M_w 6.4 or M_w 7.1 earthquakes as the
 191 autocorrelation procedure is less effective for these large earthquakes, which would re-
 192 quire other approaches for detailed analyses (e.g. Ellsworth & Bulut, 2018; Yoon et al.,
 193 2019).

194 We observe immediate-foreshocks of earthquakes with magnitudes ranging from 0.9
 195 to 5.4 and find these earthquakes have a similar magnitude-frequency distribution to that
 196 of the 13,895 investigated earthquakes (Figure S6). Additionally, the immediate-foreshocks
 197 do not show characteristics that can differentiate the mainshocks of different fault seg-
 198 ments (Figure 1a). These 527 earthquakes are distributed across the whole seismogenic
 199 zone from 0 to 13 km, penetrating beyond the creeping transition depth at 11.0 km (Fig-
 200 ure 3g and see Text S3). The immediate-foreshocks generate precursory signals preced-
 201 ing the mainshock P-waves by 0.5 to 100 s. These preceding times do not seem to scale
 202 with earthquake magnitudes nor depths (Figures 3b and h). Intriguingly, amplitude ra-
 203 tios of $M \geq 2.5$ events are larger on average than those of smaller magnitude earth-
 204 quakes (Figure 1a and Figure S6c). However, the robustness of this observation is dif-
 205 ficult to verify due to fewer $M \geq 2.5$ earthquakes (total 41 events). These $M \geq 2.5$
 206 earthquakes are more likely to have higher amplitude ratios for the same noise level and
 207 detection threshold (detecting more low-amplitude precursory signals) because low am-
 208 plitude precursory signals of smaller earthquake are more likely buried in the background
 209 noise than those of larger events.

210 Using the differential times obtained from the autocorrelation procedure and a 1D
 211 average velocity model of Southern California (Lee et al., 2014), we further determine
 212 the relative locations between the 527 earthquakes and their immediate-foreshocks (Fig-
 213 ure 4a and see Text S4). About 84% of these immediate-foreshocks are located within
 214 0.2 km of the mainshock hypocenters with a median separation of 59 m (Figure 4a). We
 215 further evaluate the relative location uncertainty by performing jackknife-resampling of
 216 the stations (Efron & Tibshirani, 1994) (Text S4). About 85% of the separation distance
 217 between the immediate-foreshocks and mainshocks has a standard deviation less than

0.1 km with a median value of 15 m horizontally (Figure S7f). Vertically, 78% of the separation distance has a standard deviation less than 0.1 km with a median value of 31 m (Figure S7f). Further, we observe more than 85% of the immediate-foreshocks occurred within 60 s of the mainshocks despite the searching window is 100 s long (Figure 4c). Without knowing the magnitudes and stress-drop estimates of the immediate-foreshocks, we cannot evaluate the static/dynamic stress perturbations at the mainshock locations from the immediate-foreshocks. However, the spatiotemporal clustering suggests that the immediate-foreshocks likely near-instantaneously triggered the following slip, indicating a rapid rupture development (Shearer & Lin, 2009; Yoon et al., 2019).

Out of the 527 earthquakes, 48 earthquakes have series of successive precursory signals, indicating a possible complex evolution of the rupture developments. For example, we identify two immediate-foreshocks for a M 2.5 earthquake (Figures 2 and S5). This sequence of precursory signals share high resemblances with the M 2.5 earthquake P-waves with an average cross-correlation coefficient of 0.91, yet their amplitudes are 127.6 and 1067.8 times smaller than the P-waves on average (Figure S5). These observations likely represent a hierarchical nucleation process that the observed earthquakes are products of a series of cascadingly triggered slip patches (Wyss & Brune, 1967; Fukao & Furumoto, 1985; Ide, 2019; Okuda & Ide, 2018; Ellsworth & Bulut, 2018; Abercrombie & Mori, 1994). These observations also suggest that the Ridgecrest fault system may have a fractal strength or stress structure over orders of scale. Characteristics of these 48 earthquakes and their immediate-foreshocks, including the earthquake location, amplitude ratio, and preceding time, show no differences to those of the rest 479 earthquakes that only have single precursors, rendering that earthquake rupture development is stochastic and local fine-scale heterogeneous fault properties control the rupture evolution (Ide, 2019; McLaskey, 2019; Ide & Aochi, 2005).

4 Discussions and Conclusions

The observed immediate-foreshocks show clear spatiotemporal correlations with the following earthquakes (Figures 4a and 4b), but are they precursors of the earthquakes or simply random forerunners? To evaluate the influence of the immediate-foreshocks in nucleating the following slip, we compare the immediate-foreshocks with cataloged earthquakes in Shelly (2020). We first investigate the spatiotemporal behaviors of all the cataloged earthquakes that are within 1 km to the 527 earthquake hypocenters, which have one or more immediate-foreshocks. The separation distance and time between two sequential cataloged earthquakes show different distributions comparing to those of the immediate-foreshocks (Figures 4c and 4d). These sequential earthquakes seem to be relatively uniformly separated in space (within 1 km), and the separation time seems to be Poissonian. Such characteristics show that the sequential earthquakes are mostly independent, random cases. In contrast, the immediate-foreshocks cluster in space and time, suggesting they are not random but more likely have influenced the following earthquakes, hence precursors.

We also compare the immediate-foreshocks with correlated seismicity in Shelly (2020), including foreshock-mainshock and mainshock-aftershock sequences (Figure S8). These sequences are defined as sequential earthquakes occurring within 1 km and 100 s and the foreshocks/aftershocks having smaller magnitudes comparing to the mainshocks (across the whole region, not just near the 527 earthquakes with immediate-foreshocks). In Shelly (2020), there are 363 foreshock-mainshock and 519 mainshock-aftershock sequences (Text S5). The separation distances between the foreshocks/aftershocks and the mainshocks show similarities with the immediate-foreshocks as they all cluster within 0.2 km of the mainshock hypocenters (Figure 4d). The separation time distributions are different (Figure 4c). There seems to be an apparent paucity of aftershocks soon after the mainshocks and most of the aftershocks seem to occur at or after 20 s of the mainshocks. The lack of aftershocks soon after the mainshocks may be due to the coda waves or noises in the records

270 (Kagan & Houston, 2005). The foreshocks in the high resolution catalog are akin to the
 271 immediate-foreshocks, i.e., clustering spatiotemporally with the mainshocks, but also show
 272 differences. Most of the foreshocks occurred more than 5 s ahead of the mainshocks, while
 273 our immediate-foreshocks peak within 5 s of the following mainshocks (Figure 4b,c). Fur-
 274 further, the occurrence of the 527 observed immediate-foreshocks and the 363 foreshocks
 275 in Shelly (2020) follow the inverse Omori’s law as there are more immediate-foreshocks
 276 and catalog foreshocks as the the mainshocks approach, but the two classes of seismic-
 277 ity grow at different rates (Figure S9 and see Text S6).

278 In most studies, the term “foreshock” is loosely defined, and they are often con-
 279 sidered in a much larger spatiotemporal scales, i.e., over ten of kilometers and/or days
 280 of periods (Abercrombie & Mori, 1996; Shearer & Lin, 2009; Chen & Shearer, 2013; Trug-
 281 man & Ross, 2019). The foreshocks that we search in the high resolution catalog (Shelly,
 282 2020) are specific events analogous to our immediate-foreshocks, and they are selected
 283 based on strict constraints in space and time (Figure 4). Therefore, the observed vari-
 284 ations of the foreshocks and immediate-foreshocks in Figure 4c may not be inconsistent
 285 but represent the same process at two resolutions. For example, characteristics of these
 286 foreshock-mainshock sequences show similar patterns as those of the observed immediate-
 287 foreshocks, and we do not find clear scaling relationships among the earthquake mag-
 288 nitude, depth, preceding time, and magnitude difference (Figure S8). Therefore, the fore-
 289 shocks in the high resolution catalog (Shelly, 2020) and the immediate-foreshocks in this
 290 study may demonstrate the same type of preparation phase for the mainshocks. Particu-
 291 larly, our immediate-foreshocks offer a high resolution view of slip events ahead of the
 292 earthquake onsets because of the spatial collocation and the short separation time. They
 293 demonstrate a near-instantaneous response of the following slip events, indicating that
 294 the mainshocks are nucleated by stress transferring from the immediate-foreshocks.

295 The current set of observations can be best explained by the cascade model (Wyss
 296 & Brune, 1967; Fukao & Furumoto, 1985; Ide & Aochi, 2005; Aochi & Ide, 2004; Lui &
 297 Lapusta, 2016). In this cascade model, a slip event on a small fault patch that is adja-
 298 cent or within the earthquake rupture area rapidly transfers stress to a surrounding fault
 299 and leads to an unsteady dynamic rupture (Ide & Aochi, 2005; Lui & Lapusta, 2016; McLaskey,
 300 2019). Such processes have been observed in earthquakes with a range of magnitudes.
 301 For example, the 1964 Mw 9.2 Alaska earthquakes was shortly preceded by a sequence
 302 of earthquakes within 100 s (likely immediate-foreshocks) before its onset, and the prop-
 303 agating rupture of the sequence eventually led to the great earthquake (Wyss & Brune,
 304 1967). The propagation of such a cascade process is controlled by the local stress and
 305 strength heterogeneities, which effectively reflect as hierarchically distributed fault patches,
 306 and naturally, the barriers between such patches determine the termination of the cas-
 307 cade process, the earthquake eventual magnitude (Fukao & Furumoto, 1985; Noda et al.,
 308 2013; Aochi & Ide, 2004; Ide & Aochi, 2005). It is worth noting that large earthquakes
 309 (e.g., $M \geq 6$) have P-waves significantly different from those of small events, therefore, we
 310 did not investigate the M_w 6.4 and the M_w 7.1 Ridgecrest earthquakes. However, fore-
 311 shocks seem to have cascadingly triggered the M_w 6.4 earthquake without evidence of
 312 observable aseismic slips (Ellsworth et al., 2020).

313 The structure of hierarchical fault patches implies multiscale heterogeneities, which
 314 is likely the physical cause of the series of successive precursory signals (Figures 2 and
 315 S5). These fault patches and heterogeneities associate with the stress distribution, fault
 316 roughness, and fault gouge, which may have developed naturally as the fault structure
 317 evolves over multiple seismic cycles (Davidesko et al., 2014; Martel et al., 1988; Trug-
 318 man et al., 2020). In particular, the 2019 Mw 7.1 Ridgecrest earthquake has caused stress
 319 variabilities on length scales of hundreds of meters or less, leading to faulting complex-
 320 ities throughout the earthquake sequence (Trugman et al., 2020). Such complex struc-
 321 tures and heterogeneities have scales comparable to those of the separation distances be-
 322 tween the immediate-foreshocks and the mainshocks (Figure 4), favoring the cascade nu-

323 cleation process. Previous numerical studies show that the rate-and-state friction law
324 and a set of randomly distributed fractal fault patches can produce a wide variety of cas-
325 cading rupture scenarios for both small and large earthquakes (Fukao & Furumoto, 1985;
326 Ide, 2019). Furthermore, recent laboratory experiments suggest a rate-dependent cas-
327 cade process that may have been facilitated by the varying nucleation length in addi-
328 tion to the fault property heterogeneities (McLaskey, 2019). These studies suggest that
329 the final magnitude is the only difference between small and large earthquakes. For the
330 Ridgecrest earthquakes, the lack of scaling relations between the precursory signals and
331 the P-waves and the diverse characteristics of the immediate-foreshocks indicate such
332 a stochastic rupture development and support the cascade model (Figure 3). Our results
333 concur that earthquakes nucleate in a similar fashion and large events are simply results
334 of favorable continuous rupture conditions. For example, the M 3.9 and the M_w 5.4 earth-
335 quakes occurred within 2.6 km and have similar precursory signals (SCEDC; Hutton et
336 al., 2010), but the final moments were 165 times different (Figures 2, S1–2, and S4). Such
337 disparities emphasize that fine-scale heterogeneities or barriers modulate earthquake rup-
338 ture development in complex ways.

339 Another possible nucleation mechanism is the preslip model (Ellsworth & Beroza,
340 1995; McLaskey, 2019; Dodge et al., 1996). In this model, the final earthquake magni-
341 tude correlates with the aseismic slip size, which can trigger foreshocks but the foreshocks
342 do not prepare the following mainshocks. Therefore, this model hints that the aseismic
343 nucleation characteristics would affect the later stage rupture of an earthquake, although
344 seismic observations of the preslip model may be indistinguishable from those caused by
345 the cascade model (Ellsworth & Beroza, 1995). Recent observations of some large sub-
346 duction zone earthquakes can be explained by this model (Kato et al., 2012; Ruiz et al.,
347 2014, 2017). The preslip model would suggest that earthquake nucleation preferentially
348 occurs at the transition zones between the creeping and locked fault segments and a co-
349 alescence of seismicity would migrate around the earthquake epicenter for some extended
350 period before the fault slip reaching a critical nucleation length (Lapusta & Rice, 2003;
351 Tape et al., 2018). In our observations, earthquakes with immediate-foreshocks occurred
352 at all depths beyond the transition zone, and we rarely observe more than one precur-
353 sory signals for a given earthquake. However, additional precursory signals may have been
354 missed by our autocorrelation procedure, which is less effective at detecting aseismic slips
355 or slip events that are away from the earthquake hypocenter. It is possible that multi-
356 ple processes have occurred concurrently and have modulated the nucleation process as
357 a rate-dependent feedback system, which has been documented in experiments, simu-
358 lations, and field observations (McLaskey, 2019; Lapusta & Rice, 2003; Yao et al., 2020).

359 We do not observe seismic precursory signals for every investigated earthquake. Roughly,
360 4% of the 13,895 earthquakes have identifiable immediate-foreshocks. This is likely lim-
361 ited by the data as the majority of the immediate-foreshocks are inferred from the nodal
362 array data, and the precursory signals are often buried in noise at the regional network
363 stations. It is also possible that there are more immediate-foreshocks but their separa-
364 tion times are too short to be resolved by our current procedure or available data. Ad-
365 ditionally, our procedure may have excluded seismic precursory signals beyond the 100 s
366 time window that we have scanned through. In this case, there might be other prepa-
367 ration processes than the near-instantaneous stress transferring nucleation as demonstrated
368 by the immediate-foreshocks. Finally, our observations only represent one class of the
369 earthquake nucleation processes and there are other physical mechanisms initiating the
370 Ridgecrest earthquakes in addition to the aforementioned end-member models. Never-
371 theless, the immediate-foreshocks highlights the importance of near-field observations,
372 in particular, the needs of fault-zone observations.

373 Whether the growth trajectory of an earthquake can be robustly forecasted depends
374 on understanding the influences of the earthquake precursors over the later stage rup-
375 ture (Meier et al., 2017; McLaskey, 2019; Mori & Kanamori, 1996; Iio, 1992). Fine-scale

376 rate-dependent physical processes, e.g., grain crushing, microcracking, and plastic de-
 377 formation, may have strong impacts on the earthquake rupture development (Yamashita,
 378 2000; Xu et al., 2019). Such processes are challenging to measure geophysically and can-
 379 not be deterministically predicted, which may cause small and large earthquakes show-
 380 ing similar seismic precursors.

381 For the Ridgecrest earthquakes, we find abundant immediate-foreshocks for earth-
 382 quakes with magnitude from 0.9 to 5.4 that may have helped nucleating the earthquakes.
 383 Numerous earthquakes occurred in the same region showing similar seismic precursory
 384 signals but developed into events with different eventual magnitudes, illuminating the
 385 limited predictability of the earthquake growth process (Figure 3). For instance, we find
 386 that there is no scaling relationship between the amplitude ratio or the preceding time
 387 with the earthquake magnitude (Figures 3a and b). However, we find that all the ob-
 388 served immediate-foreshocks occurred within 100 s of the earthquakes with a temporal
 389 clustering around 7 seconds and 0.06 km (Figure S10). This time-distance clustering of
 390 the 527 earthquakes and their immediate-foreshocks shows a possible common prepa-
 391 ration process that nucleate earthquakes near-instantaneously in the Ridgecrest fault sys-
 392 tem.

393 **Data Availability Statement**

394 The 13,895 earthquakes investigated in the study are from the Southern California Earth-
 395 quake Data Center catalog (SCEDC; Hutton et al., 2010). The high resolution catalog
 396 used for comparison is from Shelly (2020). The seismic records were provided by Data
 397 Management Center (DMC) of the Incorporated Research Institutions for Seismology
 398 (IRIS) and the SCEDC (Caltech.Dataset., 2013). The nodal array data is openly avail-
 399 able through IRIS DMC and was acquired by the U.S. Geological Survey (USGS) (Catchings
 400 et al., 2020), the Southern California Earthquake Center (SCEC), and SCEC member
 401 institutions. The 1D velocity model used in this study is obtained from averaging the
 402 community velocity model of Southern California (Lee et al., 2014). The earthquakes
 403 that have immediate-foreshocks are listed in Table S1.

404 **Acknowledgments**

405 The research was supported by NSF EAR-2022441 and by the Southern California Earth-
 406 quake Center (SCEC; Award No. 20115 and Contribution No. 10957). SCEC is funded
 407 by NSF Cooperative Agreement EAR-1600087 & USGS Cooperative Agreement G17AC00047.
 408 We thank the editor Dr. Prieto, AE Dr. Tsai, Dr. Trugman, an anonymous reviewer,
 409 Dr. Shearer, Dr. Barbour, and Dr. McGuire for their insightful, constructive suggestions,
 410 which have led to improvements in the paper.

411 **References**

- 412 Abercrombie, R. E., & Mori, J. (1994). Local observations of the onset of a large
 413 earthquake: 28 June 1992 Landers, California. *Bulletin of the Seismological So-*
 414 *ciety of America*, *84*(3), 725–734.
- 415 Abercrombie, R. E., & Mori, J. (1996). Occurrence patterns of foreshocks to large
 416 earthquakes in the western united states. *Nature*, *381*(6580), 303–307.
- 417 Aochi, H., & Ide, S. (2004). Numerical study on multi-scaling earthquake rupture.
 418 *Geophysical research letters*, *31*(2).
- 419 Ben-Zion, Y., Katz, S., & Leary, P. (1992). Joint inversion of fault zone head waves
 420 and direct P arrivals for crustal structure near major faults. *Journal of Geo-*
 421 *physical Research: Solid Earth*, *97*(B2), 1943–1951.
- 422 Ben-Zion, Y., & Malin, P. (1991). San Andreas fault zone head waves near Parkfield,
 423 California. *Science*, *251*(5001), 1592–1594.
- 424 Beroza, G. C., & Ellsworth, W. L. (1996). Properties of the seismic nucleation
 425 phase. *Tectonophysics*, *261*(1-3), 209–227.

- 426 Bolton, D. C., Shokouhi, P., Rouet-Leduc, B., Hulbert, C., Rivière, J., Marone, C.,
427 & Johnson, P. A. (2019). Characterizing acoustic signals and searching for
428 precursors during the laboratory seismic cycle using unsupervised machine
429 learning. *Seismological Research Letters*, *90*(3), 1088–1098.
- 430 Bouchon, M., Durand, V., Marsan, D., Karabulut, H., & Schmittbuhl, J. (2013).
431 The long precursory phase of most large interplate earthquakes. *Nature Geo-*
432 *science*, *6*(4), 299–302. doi: 10.1038/ngeo1770
- 433 Caltech.Dataset. (2013). Southern California Earthquake Data Center.
434 doi: 10.7909/C3WD3xH1
- 435 Catchings, R. D., Goldman, M., Steidl, J., Chan, J., Allam, A., Criley, C., . . . Ben-
436 Zion, Y. (2020). Nodal seismograph recordings of the 2019 Ridgecrest earth-
437 quake sequence. *Seismological Research Letters*, *91*(6), 3622–3633.
- 438 Chen, X., & Shearer, P. M. (2013). California foreshock sequences suggest aseismic
439 triggering process. *Geophysical Research Letters*, *40*(11), 2602–2607.
- 440 Cochran, E. S., Wolin, E., McNamara, D. E., Yong, A., Wilson, D., Alvarez, M., . . .
441 Steidl, J. (2020). The U.S. Geological Survey’s rapid seismic array deployment
442 for the 2019 Ridgecrest Earthquake Sequence. *Seismological Research Letters*,
443 *91*(4), 1952–1960. doi: 10.1785/0220190296
- 444 Davidesko, G., Sagy, A., & Hatzor, Y. H. (2014). Evolution of slip surface roughness
445 through shear. *Geophysical Research Letters*, *41*(5), 1492–1498.
- 446 Dodge, D. A., Beroza, G. C., & Ellsworth, W. L. (1996). Detailed observations of
447 california foreshock sequences: Implications for the earthquake initiation pro-
448 cess. *Journal of Geophysical Research: Solid Earth*, *101*(B10), 22371–22392.
- 449 Efron, B., & Tibshirani, R. J. (1994). *An introduction to the bootstrap*. CRC press.
- 450 Ellsworth, W. L., Barbour, A. J., & Shelly, D. R. (2020). Foreshock cascade to fail-
451 ure in the m_w 6.4 July 4, 2019 Ridgecrest, California earthquake. *Poster Pre-*
452 *sentation at 2020 SCEC Annual Meeting*.
- 453 Ellsworth, W. L., & Beroza, G. (1995). Seismic evidence for an earthquake nucle-
454 ation phase. *Science*, *268*(5212), 851–855.
- 455 Ellsworth, W. L., & Bulut, F. (2018). Nucleation of the 1999 Izmit earthquake by a
456 triggered cascade of foreshocks. *Nature Geoscience*, *11*(7), 531–535.
- 457 Fan, W., & McGuire, J. J. (2018). Investigating microearthquake finite source
458 attributes with IRIS community wavefield demonstration experiment in Okla-
459 homa. *Geophysical Journal International*, *214*(2), 1072–1087.
- 460 Fukao, Y., & Furumoto, M. (1985). Hierarchy in earthquake size distribution.
461 *Physics of the earth and planetary interiors*, *37*(2-3), 149–168.
- 462 Goebel, T., Schorlemmer, D., Becker, T., Dresen, G., & Sammis, C. (2013). Acous-
463 tic emissions document stress changes over many seismic cycles in stick-slip
464 experiments. *Geophysical Research Letters*, *40*(10), 2049–2054.
- 465 Huang, H., Meng, L., Bürgmann, R., Wang, W., & Wang, K. (2020). Spatio-
466 temporal foreshock evolution of the 2019 M 6.4 and M 7.1 Ridgecrest, Califor-
467 nia earthquakes. *Earth and Planetary Science Letters*, *551*, 116582.
- 468 Hutton, K., Woessner, J., & Hauksson, E. (2010). Earthquake monitoring in south-
469 ern California for seventy-seven years (1932–2008). *Bulletin of the Seismologi-*
470 *cal Society of America*, *100*(2), 423–446.
- 471 Ide, S. (2019). Frequent observations of identical onsets of large and small earth-
472 quakes. *Nature*, *573*(7772), 112–116.
- 473 Ide, S., & Aochi, H. (2005). Earthquakes as multiscale dynamic ruptures with het-
474 erogeneous fracture surface energy. *Journal of Geophysical Research: Solid*
475 *Earth*, *110*(B11).
- 476 Iio, Y. (1992). Slow initial phase of the P-wave velocity pulse generated by mi-
477 croearthquakes. *Geophysical research letters*, *19*(5), 477–480.
- 478 Jin, Z., & Fialko, Y. (2020). Finite slip models of the 2019 Ridgecrest earthquake se-
479 quence constrained by space geodetic data and aftershock locations. *Bulletin of*
480 *the Seismological Society of America*, *110*(4), 1660–1679.

- 481 Johnson, P. A., Ferdowski, B., Kaproth, B. M., Scuderi, M., Griffa, M., Carmeliet, J.,
 482 ... Marone, C. (2013). Acoustic emission and microslip precursors to stick-slip
 483 failure in sheared granular material. *Geophysical Research Letters*, *40*(21),
 484 5627–5631.
- 485 Kagan, Y. Y., & Houston, H. (2005). Relation between mainshock rupture process
 486 and omori's law for aftershock moment release rate. *Geophysical Journal Inter-*
 487 *national*, *163*(3), 1039–1048.
- 488 Kanamori, H. (2003). Earthquake prediction: an overview. *International Geophysics*,
 489 *81*(PART B), 1205–1216. doi: 10.1016/S0074-6142(03)80186-9
- 490 Kanamori, H., & Cipar, J. J. (1974). Focal process of the great Chilean earthquake
 491 May 22, 1960. *Physics of the Earth and Planetary Interiors*, *9*(2), 128–136.
 492 doi: 10.1016/0031-9201(74)90029-6
- 493 Kato, A., Obara, K., Igarashi, T., Tsuruoka, H., Nakagawa, S., & Hirata, N. (2012).
 494 Propagation of slow slip leading up to the 2011 Mw 9.0 Tohoku-Oki earth-
 495 quake. *Science*, *335*(6069), 705–708. doi: 10.1126/science.1215141
- 496 Kilb, D., Gombert, J., & Bodin, P. (2000). Triggering of earthquake aftershocks by
 497 dynamic stresses. *Nature*, *408*(6812), 570–574.
- 498 Lapusta, N., & Rice, J. R. (2003). Nucleation and early seismic propagation of
 499 small and large events in a crustal earthquake model. *Journal of Geophysical*
 500 *Research: Solid Earth*, *108*(B4).
- 501 Lee, E.-J., Chen, P., Jordan, T. H., Maechling, P. B., Denolle, M. A., & Beroza,
 502 G. C. (2014). Full-3-D tomography for crustal structure in southern California
 503 based on the scattering-integral and the adjoint-wavefield methods. *Journal of*
 504 *Geophysical Research: Solid Earth*, *119*(8), 6421–6451.
- 505 Liu, Y., McGuire, J. J., & Behn, M. D. (2020). Aseismic transient slip on the Gofar
 506 transform fault, East Pacific Rise. *Proceedings of the National Academy of Sci-*
 507 *ences*, *117*(19), 10188–10194.
- 508 Lui, S. K., & Lapusta, N. (2016). Repeating microearthquake sequences interact pre-
 509 dominantly through postseismic slip. *Nature communications*, *7*(1), 1–7.
- 510 Marone, C. (1998). Laboratory-derived friction laws and their application to seismic
 511 faulting. *Annual Review of Earth and Planetary Sciences*, *26*(1), 643–696.
- 512 Martel, S. J., Pollard, D. D., & Segall, P. (1988). Development of simple strike-
 513 slip fault zones, Mount Abbot quadrangle, Sierra Nevada, California. *Geologi-*
 514 *cal Society of America Bulletin*, *100*(9), 1451–1465.
- 515 McGuire, J. J. (2004). Estimating finite source properties of small earthquake rup-
 516 tures. *Bulletin of the Seismological Society of America*, *94*(2), 377–393. doi: 10
 517 .1785/0120030091
- 518 McGuire, J. J. (2017). A MATLAB toolbox for estimating the second moments of
 519 earthquake ruptures. *Seismological Research Letters*, *88*(2A), 371–378. doi: 10
 520 .1785/0220160170
- 521 McLaskey, G. C. (2019). Earthquake initiation from laboratory observations and
 522 implications for foreshocks. *Journal of Geophysical Research: Solid Earth*,
 523 *124*(12), 12882–12904.
- 524 McLaskey, G. C., & Lockner, D. A. (2014). Preslip and cascade processes initiat-
 525 ing laboratory stick slip. *Journal of Geophysical Research: Solid Earth*, *119*(8),
 526 6323–6336.
- 527 McLaskey, G. C., & Yamashita, F. (2017). Slow and fast ruptures on a laboratory
 528 fault controlled by loading characteristics. *Journal of Geophysical Research:*
 529 *Solid Earth*, *122*(5), 3719–3738.
- 530 Meier, M.-A., Ampuero, J., & Heaton, T. H. (2017). The hidden simplicity of sub-
 531 duction megathrust earthquakes. *Science*, *357*(6357), 1277–1281.
- 532 Meng, H., McGuire, J. J., & Ben-Zion, Y. (2020). Semiautomated estimates of direc-
 533 tivity and related source properties of small to moderate southern California
 534 earthquakes using second seismic moments. *Journal of Geophysical Research:*
 535 *Solid Earth*, *125*(4), e2019JB018566.

- 536 Mignan, A. (2012). Seismicity precursors to large earthquakes unified in a stress
537 accumulation framework. *Geophysical Research Letters*, *39*(21), 1–5. doi: 10
538 .1029/2012GL053946
- 539 Mignan, A. (2014). The debate on the prognostic value of earthquake foreshocks: a
540 meta-analysis. *Scientific reports*, *4*, 4099.
- 541 Mori, J., & Kanamori, H. (1996). Initial rupture of earthquakes in the 1995 Ridge-
542 crest, California sequence. *Geophysical Research Letters*, *23*(18), 2437–2440.
- 543 Moutote, L., Marsan, D., Lengliné, O., & Duputel, Z. (2020). Low significance of
544 foreshock activity in southern California.
- 545 Noda, H., Nakatani, M., & Hori, T. (2013). Large nucleation before large earth-
546 quakes is sometimes skipped due to cascade-up implications from a rate and
547 state simulation of faults with hierarchical asperities. *Journal of Geophysical
548 Research: Solid Earth*, *118*(6), 2924–2952.
- 549 Ohnaka, M. (1992). Earthquake source nucleation: a physical model for short-term
550 precursors. *Tectonophysics*, *211*(1-4), 149–178.
- 551 Okuda, T., & Ide, S. (2018). Hierarchical rupture growth evidenced by the initial
552 seismic waveforms. *Nature communications*, *9*(1), 1–7.
- 553 Pritchard, M. E., Allen, R. M., Becker, T. W., Behn, M. D., Brodsky, E. E.,
554 Bürgmann, R., ... others (2020). New opportunities to study earthquake
555 precursors. *Seismological Research Letters*, *91*(20), 2444–2447.
- 556 Renard, F., Cordonnier, B., Kobchenko, M., Kandula, N., Weiss, J., & Zhu, W.
557 (2017). Microscale characterization of rupture nucleation unravels precursors
558 to faulting in rocks. *Earth and Planetary Science Letters*, *476*, 69–78.
- 559 Renard, F., Weiss, J., Mathiesen, J., Ben-Zion, Y., Kandula, N., & Cordonnier, B.
560 (2018). Critical evolution of damage toward system-size failure in crystalline
561 rock. *Journal of Geophysical Research: Solid Earth*, *123*(2), 1969–1986.
- 562 Ross, Z. E., Idini, B., Jia, Z., Stephenson, O. L., Zhong, M., Wang, X., ... Moore,
563 A. W. (2019). Hierarchical interlocked orthogonal faulting in the 2019 Ridge-
564 crest earthquake sequence. *Science*, *366*5(October), 346–351.
- 565 Ruiz, S., Aden-Antoniow, F., Baez, J., Otarola, C., Potin, B., del Campo, F., ...
566 others (2017). Nucleation phase and dynamic inversion of the Mw 6.9 Val-
567 paraíso 2017 earthquake in central Chile. *Geophysical Research Letters*, *44*(20),
568 10–290.
- 569 Ruiz, S., Metois, M., Fuenzalida, A., Ruiz, J., Leyton, F., Grandin, R., ... Cam-
570 pos, J. (2014). Intense foreshocks and a slow slip event preceded the
571 2014 Iquique Mw 8.1 earthquake. *Science*, *345*(6201), 1165–1169. doi:
572 10.1126/science.1256074
- 573 Seif, S., Zechar, J. D., Mignan, A., Nandan, S., & Wiemer, S. (2019). Foreshocks
574 and their potential deviation from general seismicity. *Bulletin of the Seismolog-
575 ical Society of America*, *109*(1), 1–18.
- 576 Shearer, P. M., & Lin, G. (2009). Evidence for Mogi doughnut behavior in seismicity
577 preceding small earthquakes in southern California. *Journal of Geophysical Re-
578 search: Solid Earth*, *114*(B1).
- 579 Shelly, D. R. (2020). A high-resolution seismic catalog for the initial 2019 Ridgecrest
580 earthquake sequence: foreshocks, aftershocks, and faulting complexity. *Seismo-
581 logical Research Letters*, *91*(4), 1971–1978.
- 582 Spudich, P., & Cranswick, E. (1984). Direct observation of rupture propagation dur-
583 ing the 1979 Imperial Valley earthquake using a short baseline accelerometer
584 array. *Bulletin of the Seismological Society of America*, *74*(6), 2083–2114.
- 585 Sykes, L. R., Shaw, B. E., & Scholz, C. H. (1999). Rethinking earthquake pre-
586 diction. *Pure and Applied Geophysics*, *155*(2-4), 207–232. doi: 10.1007/
587 s000240050263
- 588 Tape, C., Holtkamp, S., Silwal, V., Hawthorne, J., Kaneko, Y., Ampuero, J. P., ...
589 West, M. E. (2018). Earthquake nucleation and fault slip complexity in the
590 lower crust of central Alaska. *Nature Geoscience*, *11*(7), 536–541.

- 591 Tinti, E., Scuderi, M., Scognamiglio, L., Di Stefano, G., Marone, C., & Collettini, C.
592 (2016). On the evolution of elastic properties during laboratory stick-slip ex-
593 periments spanning the transition from slow slip to dynamic rupture. *Journal*
594 *of Geophysical Research: Solid Earth*, *121*(12), 8569–8594.
- 595 Trugman, D. T., & Ross, Z. E. (2019). Pervasive foreshock activity across southern
596 california. *Geophysical Research Letters*, *46*(15), 8772–8781.
- 597 Trugman, D. T., Ross, Z. E., & Johnson, P. A. (2020). Imaging stress and faulting
598 complexity through earthquake waveform similarity. *Geophysical Research Let-*
599 *ters*, *47*(1), e2019GL085888.
- 600 Uchide, T., & Ide, S. (2010). Scaling of earthquake rupture growth in the Parkfield
601 area: Self-similar growth and suppression by the finite seismogenic layer. *Jour-*
602 *nal of Geophysical Research: Solid Earth*, *115*(B11).
- 603 van den Ende, M. P., & Ampuero, J.-P. (2020). On the statistical significance
604 of foreshock sequences in southern california. *Geophysical Research Letters*,
605 *47*(3), e2019GL086224.
- 606 Wyss, M., & Brune, J. N. (1967). The Alaska earthquake of 28 march 1964: A com-
607 plex multiple rupture. *Bulletin of the Seismological Society of America*, *57*(5),
608 1017–1023.
- 609 Xu, S., Fukuyama, E., & Yamashita, F. (2019). Robust estimation of rupture prop-
610 erties at propagating front of laboratory earthquakes. *Journal of Geophysical*
611 *Research: Solid Earth*, *124*(1), 766–787. doi: 10.1029/2018JB016797
- 612 Yamashita, T. (2000). Generation of microcracks by dynamic shear rupture and its
613 effects on rupture growth and elastic wave radiation. *Geophysical Journal In-*
614 *ternational*, *143*(2), 395–406.
- 615 Yao, D., Huang, Y., Peng, Z., & Castro, R. R. (2020). Detailed investigation of the
616 foreshock sequence of the 2010 Mw 7.2 El Mayor-Cucapah earthquake. *Journal*
617 *of Geophysical Research: Solid Earth*, *125*(6), e2019JB019076.
- 618 Yoon, C. E., Yoshimitsu, N., Ellsworth, W. L., & Beroza, G. C. (2019). Foreshocks
619 and mainshock nucleation of the 1999 Mw 7.1 Hector Mine, california, earth-
620 quake. *Journal of Geophysical Research: Solid Earth*, *124*(2), 1569–1582.

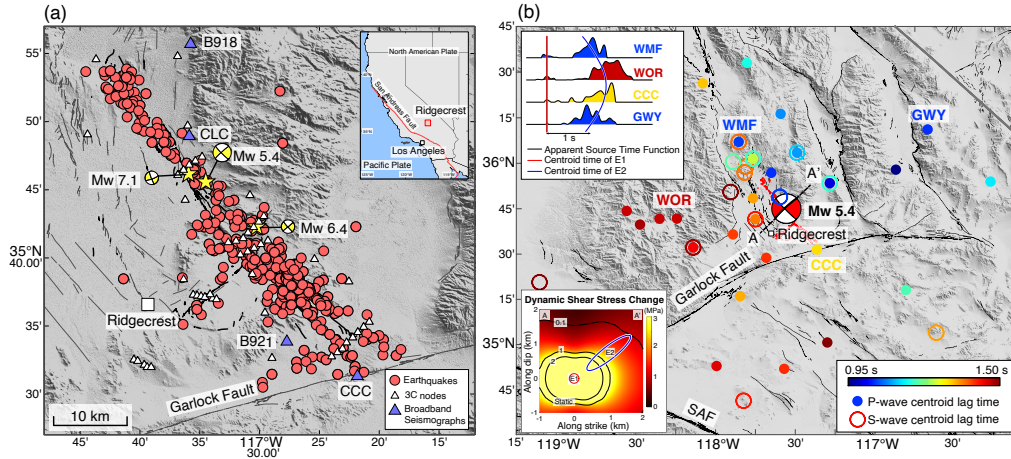


Figure 1. (a) Earthquakes with immediate-foreshocks. White triangles are the nodal stations (Catchings et al., 2020) and blue triangles are four broadband seismographs (Caltech.Dataset., 2013). Fault traces are identified from geodetic observations (Jin & Fialko, 2020). The inset shows a regional map of California. (b) The centroid lag time distribution of the two subevents of the M_w 5.4 earthquake. The earthquake rupture propagated towards the northeast direction, perpendicular to the M_w 7.1 earthquake fault strike. The top-left inset shows four example apparent source time functions of the M_w 5.4 earthquake at different azimuths. The bottom left inset shows the stress perturbations at the subevent E2 from the subevent E1 (Figure S2). The color and contour show the peak dynamic- and static-stress perturbations respectively.

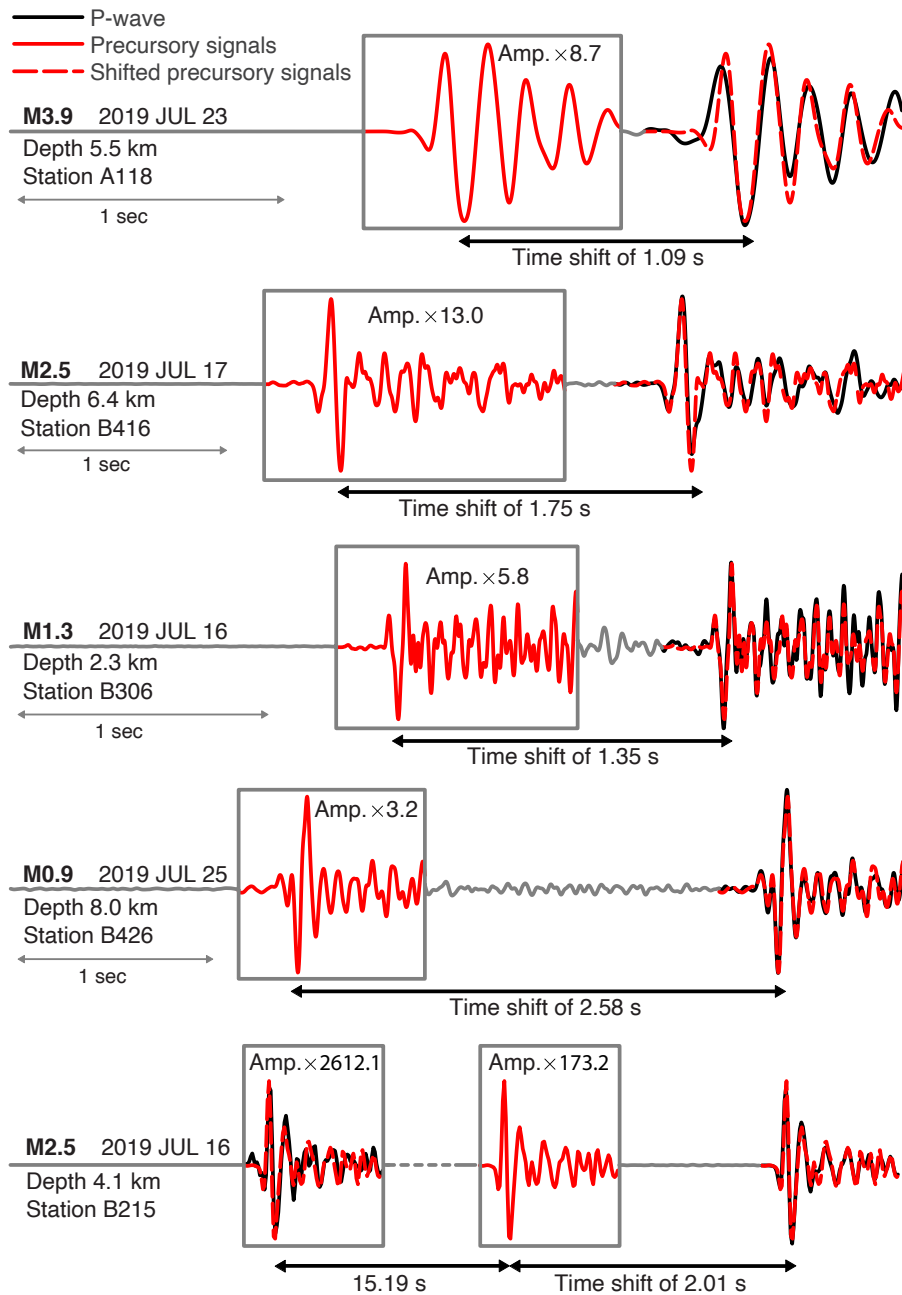


Figure 2. Example earthquake P-waves and their precursory signals from the immediate-foreshocks recorded by the nodal stations. The precursory signals are highlighted by the gray boxes and amplified for visual comparisons. The amplification factors are listed in the boxes. The records are the vertical-components of example nodal array stations and the waveforms are band-pass filtered at 1 to 20 Hz with a casual 2nd-order Butterworth filter. The amplitude ratio and preceding time distributions for each event are shown in Figures S4 and S5.

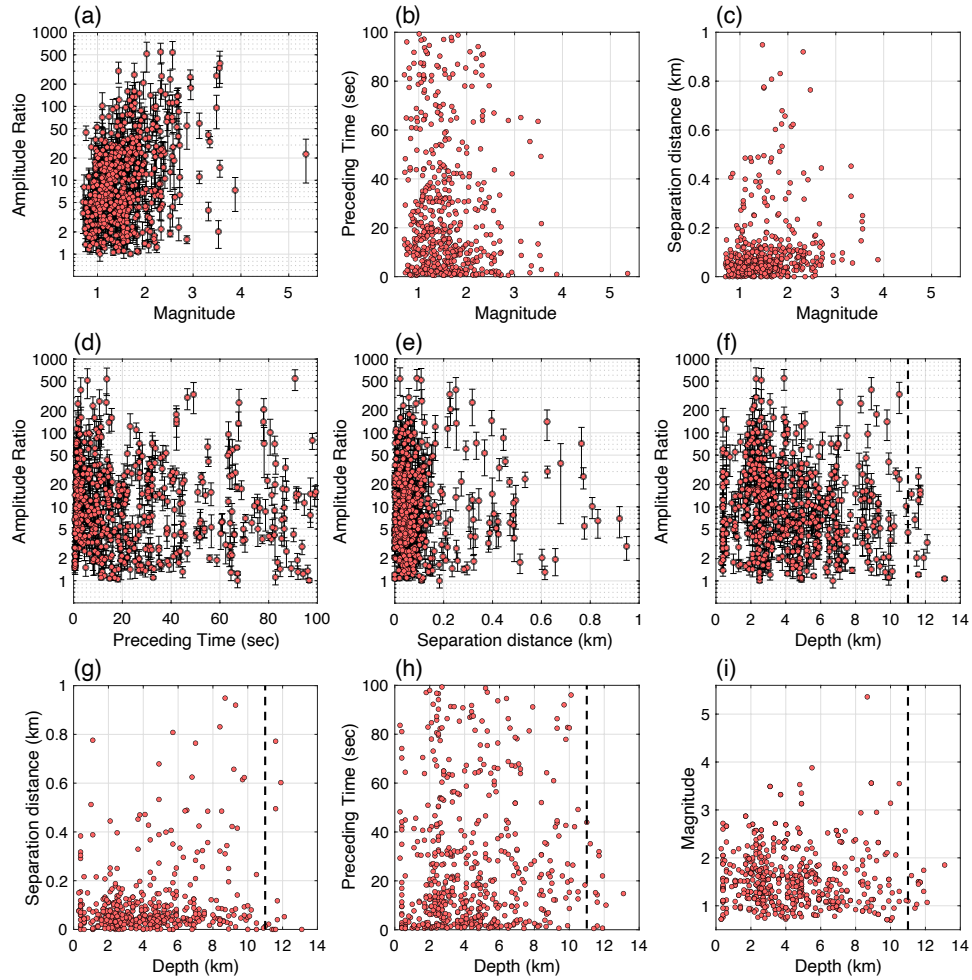


Figure 3. Scatter plots of the measured amplitude ratio, preceding time, magnitude, hypocentral separation, and depth of the earthquakes and their immediate-foreshocks. The amplitude ratio error bar shows one standard deviation of the measurements for a given earthquake. The dashed line is the 95 percentile seismicity depth, 11.0 km (Text S3).

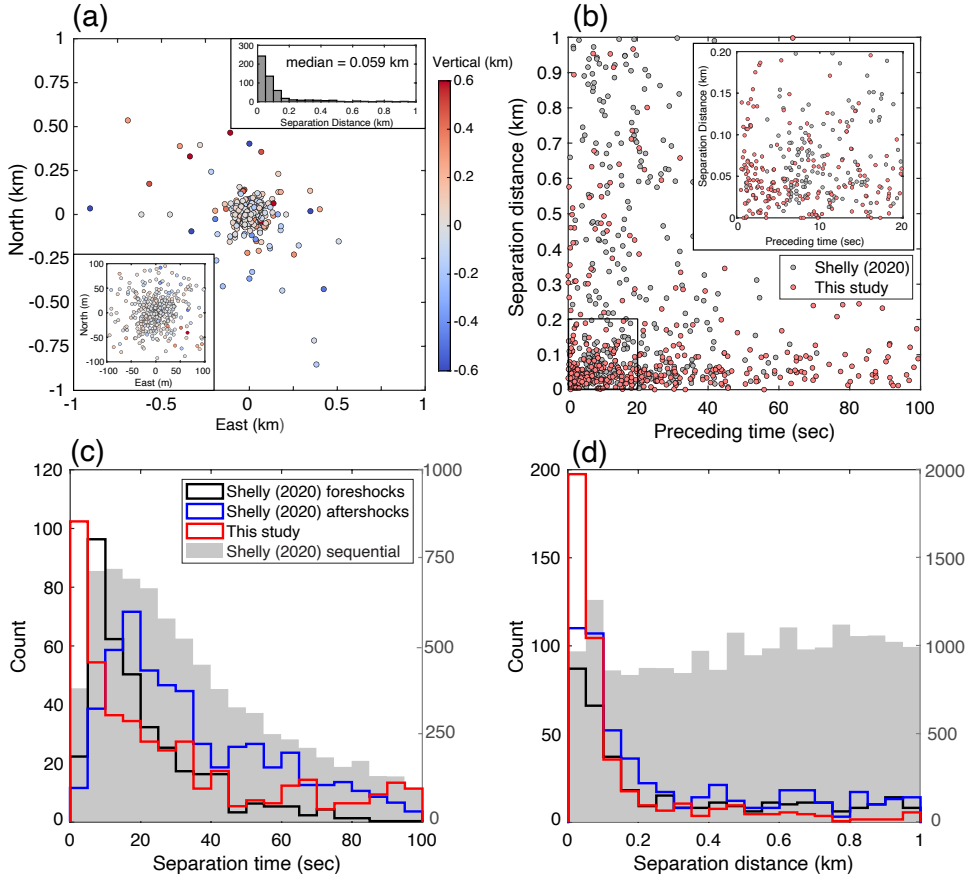


Figure 4. (a) Horizontal and vertical the separations of the immediate-foreshocks to the mainshocks. The bottom left insert shows the zoomed-in view of the hypocentral separations. The top right insert shows the histogram of separation distances with a median of 0.059 km. (b) Preceding time and separation distance of the immediate-foreshocks detected in this study and the selected foreshocks in a local high-resolution catalog (Shelly, 2020). The foreshocks are selected with preceding time less than 100 seconds and spatial separation less than 1 km of the mainshocks. (c) and (d) Distributions of separation time and distance to the mainshocks of the immediate-foreshocks detected in this study and foreshocks aftershocks in Shelly’s catalog. The foreshocks and aftershocks sequences are defined as two or more events occurring spatiotemporally within 100 s and 1 km, and the foreshock or aftershock magnitudes are smaller than those of the mainshocks. The gray histograms show the separation distance and time for sequential earthquake pairs in Shelly’s catalog within 1 km hypocentral distance of the 527 events with detected immediate-foreshocks.